A Theoretical Study of Electronic Dynamics and Deformation of CO_2 in Intense Laser Fields†

Hirohiko Kono,*,‡ Shiro Koseki,§ Masahiro Shiota,§ and Yuichi Fujimura‡

Department of Chemistry, Graduate School of Science, Tohoku University, Sendai 980-8578, Japan, and Chemistry Department for Materials, Faculty of Engineering, Mie University, Tsu 514-8507, Japan

Received: October 19, 2000; In Final Form: January 17, 2001

Deformations of CO_2, CO_2^+, and CO_2^{2+} in intense laser fields ($>10^{14}$ W/cm^2) are investigated by using potential energy surfaces of field-following adiabatic states at various instantaneous field strengths. The adiabatic states are obtained by ab initio molecular orbital calculations. To predict tunnel ionization of multi-electron molecules, we propose a new approach based on the idea that electron transfer induced by an intense laser field charges each atom in a molecule and that ionization proceeds via the most negatively (or least positively) charged atomic site. We conclude that bond stretching in CO_2^{2+} accompanied by large amplitude bending motion is responsible for the experimentally determined geometrical structure of Coulomb explosion species CO_2^{3+}, namely, that the C−O bond length is stretched to about 1.6 Å and the mean amplitude of bending is relatively large (∼40°).

1. Introduction

The development of high-power, ultrashort pulse laser technology has opened up a research field of new phenomena in intense fields such as multiphoton ionization (MPI),[1] above-threshold ionization (ATI),[2,3] and tunnel ionization.[2,4,5] As a light source for intensity $I > 10^{13}$ W/cm^2 and wavelength $\lambda > 700$ nm, the Ti: sapphire regenerative amplifier system is mainly used. In such a high-intensity and low-frequency regime, the laser electric field significantly distorts the Coulombic potential that the electrons feel; the distorted potential forms a "quasi-static" barrier (or barriers) through which an electron or electrons can tunnel.[2,4,5] This type of ionization is called tunnel ionization. The tunnel ionization regime can be distinguished by using the Keldysh parameter $\gamma = \omega\sqrt{2I_p}/f(t)$,[4] where I_P is the ionization potential of the system, ω is the laser frequency, and $f(t)$ is the pulse envelope at time t. The Keldysh parameter is the ratio of the time required for electron-tunneling through the quasistatic barrier to the optical period $1/\omega$. As the electric field is stronger and its period is longer, an electron penetrates or goes beyond the barrier(s) more easily before the phase of the field changes. The quasi-static tunneling condition is given by the inequality $\gamma < 1$, while the ordinary MPI regime is defined as $\gamma > 1$.

In the tunneling regime, a novel correlation between dissociation and tunnel ionization, known as enhanced ionization, has been discovered; the kinetic energies of fragments of a molecule are large (much greater than a few electronvolts) and consistent with Coulomb explosions of multiply charged cations at a *specific internuclear distance* R_c in the range of $\sim 2R_e$,[6] where R_e is the equilibrium internuclear distance. Numerical simulations indicate that tunnel ionization rates around R_c exceed those near R_e and those of dissociative fragments; i.e., ionization to higher-charge states is dramatically enhanced when the nuclei pass through the critical range. Enhanced ionization has been observed for various molecules[7−9] such as CO_2.[10,11] Even for ultrashort femtosecond pulses (<100 fs), hard fragmentation (small fragments are produced) is observed at higher intensity ($>10^{15}$ W/cm^2).[12]

To understand the combined process of photodissociation and photoionization, one must solve the time-dependent Schrödinger equation for molecules in intense fields. Recent accurate numerical simulations of ionization for one-electron systems such as H_2^+ and H_3^{2+} have shown that the peak ionization rate at the critical internuclear distance R_c exceeds the rate near R_e and that of the neutral fragment H by 1 or 2 orders of magnitude.[13−15] Maxima in the ionization rate with respect to the internuclear distance R have also been found for two-electron model systems such as H_2 and H_4^{2+} in one-dimensional (1D) space (in the calculations, the two electrons are allowed to move only along the molecular axis).[16] A recent 3D calculation of H_2 also predicts the existence of enhanced ionization for two-electron molecules.[17] These numerical calculations show that ionization proceeds via unstable ionic states H^-H^+ and H^+H^- created by laser-induced electron transfer between the nuclei.

Laser-induced intramolecular electronic motion, which triggers tunnel ionization, can be analyzed by means of time-dependent "field-following" adiabatic states $\{|n\rangle\}$ defined as eigenfunctions of the "instantaneous" electronic Hamiltonian $H_0(t)$ including the interaction with light.[18] To obtain $\{|n\rangle\}$, we diagonalize $H_0(t)$ by using bound eigenstates of the Born−Oppenheimer electronic Hamiltonian H_{el} at zero field as a basis set. Tunnel ionization occurs from such an adiabtic state (or from adiabatic states) to Volkov states[3,19] (quantum states of a free electron in a laser field). Intramolecular electronic motion also affects nuclear motion; e.g., after one-electron ionization from H_2, the bond distance of the resultant H_2^+ stretches on the lowest adiabatic potential surface.[20,21] Once the bond stretches to a certain distance, field-induced nonadiabatic transitions to the second lowest adiabatic state of an electronically different character take place, following which tunnel ionization proceeds.[18] In the high-intensity and low-frequency regime, field-following adiabatic potential surfaces can cross

† Part of the special issue "Edward W. Schlag Festschrift".

* Corresponding author: kono@mcl.chem.tohoku.ac.jp.
‡ Tohoku University.
§ Mie University.

10.1021/jp003848i CCC: $20.00
Published on Web 04/03/2001

each other. Field-induced nonadiabatic transitions through avoided crossing points in time and internuclear coordinate space, as well as nuclear-motion induced ones, govern the electronic and nuclear dynamics in intense fields.[18,22,23]

Laser-induced ultrafast deformation of molecular structure was experimentally investigated for various molecules such as H_2O[8] and NO_2.[9] These bent molecules experience forces that increase the probability of taking a linear structure, though the mechanism has not been clearly revealed yet. Cornaggia[10] studied the laser-induced nuclear motion of CO_2 cations on the basis of distribution patterns in the covariance map of the fragment ions carrying information on the geometrical structure of parent ions and suggested the existence of large amplitude bending motion in an intense laser field. Recently, Hishikawa et al.[11] determined the mean amplitude of bending to be 25−40° for CO_2 cations by analyzing mass-resolved momentum imaging maps for a short intense pulse (1.1 PW cm^{-2}, 100 fs, 795 nm).

It is virtually impossible to accurately solve the time-dependent Schrödinger equation of multi-electron molecules such as CO_2. In this paper, we propose a new approach that is useful in predicting the electronic and nuclear dynamics of large molecules in intense laser fields. The approach requires a knowledge of only a limited number of field-following adiabatic states, that is, potential surfaces at instantaneous field strengths and corresponding charge distributions on individual atomic sites in a molecule. While the adiabatic potential surfaces predict whether the molecule is deformed, the charge distributions can be used to estimate the possibility of tunnel ionization. In this paper, we calculate field-following adiabatic potential surfaces and charge distributions of CO_2 and its cations by using ab initio molecular orbital (MO) methods. Using the potential surfaces and charge distributions obtained, we reveal the deformation stage of CO_2 in intense laser fields.

The paper is organized as follows. In the next section, on the basis of the results of accurate numerical simulation of the electronic dynamics of H_2^+ and H_2,[18,17] we propose the electrostatic model that each atom in a molecule is charged by laser-induced electron transfer and the rule that ionization proceeds via the most negatively (or least positively) charged atomic site. In section 3, we outline the ab initio MO calculations of CO_2, CO_2^+, and CO_2^{2+}. The GAMESS suite of program codes[24] is used. In section 4, we examine the deformation of CO_2 and its cations on the basis of the electrostatic model.

2. Time-Dependent Adiabatic States and Electron Transfer between Nuclei

To accurately simulate phenomena associated with tunnel ionization of molecules, one has to solve the time-dependent Schrödinger equation for the electronic degrees of freedom of the system. We are, however, not in a position to accurately solve the time-dependent Schrödinger equation for multi-electron molecules such as CO_2. A semiquantitative approach to understand tunnel ionization of molecules has been proposed. For large polyatomic molecules such as benzene, DeWitt and Levis[25] have proposed to take into account the size of electrostatic potential surfaces, i.e., extensive electron delocalization. The maximum length of the electronic dimension increases from benzene to anthracene, which results in decreasing barrier to tunnel ionization. On going from benzene to anthracene, transition from an MPI-dominated regime to a tunnel ionization-dominated regime is observed. In this paper, we provide a new approach that is useful in predicting the *electronic* and *nuclear* dynamics of molecules in intense laser fields.

The adiabatic state picture of two typical phenomena in intense laser fields, electron localization in H_2^+ [18] and electron transfer in H_2,[17,26] allows us to use a simple electrostatic model where each atom of a molecule is characterized by its excess charge due to field-induced electrons.[27,28] Such an electrostatic consideration leads to the idea that ionization proceeds via the most unstable atomic site, i.e., the most negatively (or least positively) charged atomic site. In what follows, on the basis of accurate numerical simulation of the electronic dynamics of H_2^+ and H_2, we elucidate the above idea which is applicable to multi-electron molecules such as CO_2.

We have been developing an efficient grid method, the dual transformation method,[17,29,30] to propagate the electronic wave packet accurately. In this method, we transform both the wave function and the Hamiltonian consistently to overcome the numerical difficulties arising from the divergence of the Coulomb potentials. The transformed wave function is required to be analytic so that the finite difference method works well. We have applied the method to small molecular systems such as H_2^+ [18,30] and H_2.[17] The time-dependent electronic wave function calculated is then mapped onto field-following adiabatic states. The vibrational degree of freedom is also incorporated in the calculation of H_2^+ without resorting to the Born−Oppenheimer approximation.[18] Laser-induced nuclear motion, as well as dynamics of bound electrons and the subsequent ionization process, can be understood by analyzing the time-dependent populations of adiabatic states.

The electronic dynamics of H_2^+ prior to tunnel ionization is determined by the radiative coupling between the highest occupied molecular orbital (HOMO) and the lowest unoccupied molecular orbital (LUMO), $1s\sigma_g$ and $2p\sigma_u$, respectively.[13,14,18] The transition dipole moment between them, parallel to the molecular axis, increases as $R/2$. This large transition moment is characteristic of a charge resonance transition between a bonding and a corresponding antibonding molecular orbital, which was originally pointed out by Mulliken.[31] The strong radiative coupling of the charge resonance transition changes the potential surfaces of $1s\sigma_g$ and $2p\sigma_u$ to "field-following" time-dependent adiabatic surfaces, i.e., $E_{\mp}(R) \approx -I_p(H) \mp \epsilon(t)R/2$,[18] where $\epsilon(t)$ is the laser electric field at time t and $I_p(H)$ is the ionization potential of H. The eigenvalues $E_{\pm}(R)$ and corresponding eigenstates $|+\rangle$ and $|-\rangle$ of the instantaneous Hamiltonian $H_0(t)$ are obtained by using two bound eigenstates $1s\sigma_g$ and $2p\sigma_u$ of the Born−Oppenheimer electronic Hamiltonian H_{el} of H_2^+.[32]

The instantaneous electrostatic potential for the electron in H_2^+ has two wells around the nuclei. The dipole interaction energy for an electron is $\epsilon(t)R/2$ at the right nucleus and $-\epsilon(t)R/2$ at the left nucleus. As $\epsilon(t)$ increases from zero, the potential well formed around the right nucleus ascends and the well formed around the left nucleus descends.[18] Therefore, the ascending and descending wells yield the adiabatic energies E_+ and E_-, respectively. There exist barriers between the two wells and outside the descending well. While E_- is usually below the barrier heights, E_+ can be higher than the barrier heights in the range $R_c = 7-8$ au.[15] In this critical range of R, the upper adiabatic state $|+\rangle$ is easier to ionize than is $|-\rangle$. The range of R_c values is consistent with the numerical simulations of ionization.[13,14]

After one-electron ionization from H_2, the bond distance of the resultant H_2^+ stretches on the E_- laser-induced dissociative potential (bond softening due to the laser field)[20,21] and then ionization proceeds via the $|+\rangle$ state, which is nonadiabatically created around R_c from $|-\rangle$ when the field $\epsilon(t)$ changes its sign,

i.e., when the two adiabatic potential surfaces come closest to each other. This mechanism of enhanced ionization has been directly proved by monitoring the populations of field-following adiabatic states such as $|+\rangle$ and $|-\rangle$.[18] As the field strength approaches a local maximum, a clear reduction in the population of $|+\rangle$ is observed, whereas the population of $|-\rangle$ changes very little. A nonadiabatic transition between $|+\rangle$ and $|-\rangle$ corresponds to the spatial localization of the electron near a nucleus. Enhanced ionization in H_2^+ is due to electron localization, i.e., the suppression of electron transfer between the nuclei (called charge resonance enhanced ionization[13,15]).

The above analysis based on the change in the populations of *two* adiabatic states $|+\rangle$ and $|-\rangle$ is validated by the following consideration. We have tested cases in which $H_0(t)$ is diagonalized by using the four eigenstates of H_{el}, $2s\sigma_g$, $3p\sigma_u$, $3d\sigma_g$, and $4f\sigma_u$ in addition to $1s\sigma_g$ and $2p\sigma_u$.[33] The total population of the resultant six adiabatic states is nearly equal to the sum of the populations of $|+\rangle$ and $|-\rangle$. This means that among the bound states of H_{el} only two states $1s\sigma_g$ and $2p\sigma_u$ (or $|-\rangle$ and $|+\rangle$) are mainly populated before ionization. We suggest that in the intense and low frequency regime only a limited number of basis functions or adiabatic states are required to describe the bound state dynamics prior to ionization.

Numerical simulations have shown that enhanced ionization occurs also for two-electron molecules such as 1D and 3D H_2. The existence of similar R_c's as in one-electron molecules indicates that enhanced ionization is a universal phenomenon. For the case of two-electron molecules, however, different mechanisms can be expected because the two electrons are forced to move in a correlative way by a laser field. In a previous paper,[26] we analyzed the ionization process of 1D H_2 in an intense, low-frequency laser field (intensity $I \geq 10^{14}$ W/cm^2 and $\lambda = 1064$ nm) by numerically solving the time-dependent Schrödinger equation.

According to the 1D model calculation, the laser field forces the two electrons to stay near a nucleus for a half cycle, and resultant unstable localized ionic structures such as H^-H^+ and H^+H^- are the main doorway states to tunnel ionization. An excited ionic state can cross the covalent ground-state H·H in field-following adiabatic energy. As R decreases, the population of the H^-H^+ created increases; on the other hand, with decreases in R, the ionization rate from a pure H^-H^+ structure decreases owing to the stronger attraction by the distant nucleus. As a result, the rate has a peak at the critical distance $R_c \approx 6$ au. The role of ionic states as doorway states to ionization is also confirmed in numerical simulations of 3D H_2; e.g., Saenz has calculated adiabatic state energies and their ionization rates in static fields.[34] In a wave packet simulation of 3D H_2,[17] the formation of the localized ionic state in an alternating field is confirmed and the structure is identified with the H^- anion at the nucleus around which the dipole interaction energy becomes lower (which we call the descending well in H_2).

At relatively large R ($>R_e$), the field strength necessary for creating a localized ionic state H^-H^+, ϵ_c, is estimated as follows. The energy of the initial covalent-character-dominated state H·H is roughly estimated as (atomic units are used for the equations)

$$E(\mathrm{H{\cdot}H}) \approx -2I_p(\mathrm{H}) \tag{1}$$

The energy of the localized ionic state in the descending well at the field $\epsilon(t)$, $E(H^-H^+)$, is

$$E(\mathrm{H^-H^+}) \approx -I_p(\mathrm{H}) - I_p(\mathrm{H^-}) - 1/R - |\epsilon(t)|R \tag{2}$$

where $I_p(H^-)$ is the ionization potential of H^-, $-1/R$ is the energy of the Coulomb attraction between H^- and H^+, and $-|\epsilon(t)|R$ is the dipole interaction energy of the two electrons in the descending well. The field strength ϵ in atomic units is related to the intensity I as $I = 3.5 \times 10^{16}\,\epsilon^2$ W/cm^2. A necessary condition for the formation of a localized ionic state is then given by $E(H^-H^+) < E(H{\cdot}H)$. We thus have the critical intensity ϵ_c as[17,26]

$$\epsilon_c = [I_p(\mathrm{H}) - I_p(\mathrm{H^-}) - 1/R]/R \tag{3}$$

For 3D H_2 at $R = 4$ au, one obtains $\epsilon_c \approx 0.06$ au [$I_p(H^-) = 0.028$ au $= 0.75$ eV]. As the field strength goes beyond ϵ_c, the H^-H^+ population dramatically increases, as shown in the 3D wave packet simulation.[17] The validity of the crossing condition (3) is also confirmed by identifying crossing points between field-following adiabatic potential surfaces,[26] except a region near R_e where the large gap of the avoided crossing makes it difficult to identify the crossing point.

It should be emphasized that the covalent-character-dominated initial state H·H is adiabatically connected with the lowering ionic state H^-H^+ (or H^+H^-) when these two states cross each other[26, 34] (we ignore Rydberg-like diffuse states which may be created only at extremely low frequencies). At small R, the time evolution from the ground state follows the adiabatic sequence between the covalent-character-dominated state and the ionic-character-dominated state; i.e., the bound component of the wave packet $\psi(t)$ (the projection of $\psi(t)$ onto the bound eigenstates of H_{el}) stays on the lowest adiabatic potential surface. As $|\epsilon(t)|$ goes beyond ϵ_c ($\lambda > 700$ nm), the population of H^- dramatically increases. On the other hand, at large R, the main character is always covalent; i.e., near the crossing, the initial covalent state is nonadiabatically transferred to the diabatically connected covalent state after the crossing, namely, the second lowest state after the crossing. The diabatic character originates from the fact that it takes a long time for an electron to transfer to the distant nucleus.

For H_2, tunnel ionization is governed by the population of the localized ionic components H^-H^+ and H^+H^- and by the distance between the positive and negative charges. The present consideration supports the idea that each atom in a molecule is charged by electron transfer in intense laser fields and ionization proceeds via the most unstable atomic site. If a localized ionic component is created, its ionization rate increases as the distance between the opposite charges increases. When the internuclear distance R is small, electron transfer will occur adiabatically in the time-dependent lowest adiabatic state.

3. MO Calculation of Electronic States at Instantaneous Field Strengths

To apply the simple electrostatic idea in section 2 to the CO_2 case, one needs to know adiabatic potential surfaces and charge distributions which determine, respectively, the nuclear dynamics and ionization dynamics in the intense laser field. For H_2^+ and H_2, various representations such as the grid representation in scaled cylindrical coordinates[17,29,30] and the polynomial expansion in spheroidal or elliptic coordinates[34,35] are used to calculate adiabatic potential surfaces and charge distributions. For the two-electron molecule H_2, electron correlation can be fully taken into account. Another approach, which is more practical for multi-electron molecules, are ab initio MO methods. We have found that field-following adiabatic potential surfaces and charge distributions of H_2 calculated by ab initio MO methods are in good agreement with the corresponding exact

ones. In this paper, we employ two ab initio MO methods, the multiconfiguration self-consistent-field (MCSCF) method and the full valence configuration interaction (CI) method, to calculate field-following adiabatic states of CO_2 and its cations. Comparing the two results is necessary to estimate how properly electron correlation in a field is treated.

Coulomb explosion in CO_2 starts with the fragmentation of the triply charged ion CO_2^{3+} as $O^+ + C^+ + O^+$. The determined structural parameter of the Coulomb explosion species CO_2^{3+} is as follows:[11] The C−O bond length is about 1.6 Å and the mean amplitude of bending motion is about 40° (12.5° for the ground vibrational level of the $\tilde{X}^1\Sigma_g$ state of neutral CO_2). We assume that Coulomb explosion of CO_2^{3+} begins soon after the ionization of CO_2^{2+} and the initial structure of the CO_2^{3+} in the Coulomb explosion channel is similar to the structure of the CO_2^{2+} just before ionization. In this paper, we examine the neutral, cation, and dication stages of CO_2 leading to the creation of CO_2^{3+}. The deformations of CO_2, CO_2^+, and CO_2^{2+} are investigated by using adiabatic potential surfaces of the three species at various instantaneous field strengths. Only symmetric stretching is considered; at zero field, the molecule maintains C_{2v} symmetry while bending.

All ab initio molecular orbital (MO) calculations have been performed using the GAMESS suite of program codes.[24] The full-optimized reaction space MCSCF method[36] with the 6-311+G(d) basis set[37] is employed to describe the ground state $^1\Sigma_g$ of linear CO_2 at zero field and $^1A_1$ of bent CO_2 under C_{2v}. The MCSCF active space includes all valence orbitals (12) and valence electrons (16) of CO_2. When an instantaneous field is applied along the molecular axis, the adiabatic electronic energy is calculated by the simple CI method using the MCSCF orbitals obtained at zero field. For nonzero field cases, we furthermore optimize the MOs and the expansion coefficients of the configuration state functions by the MCSCF method. Although the latter method is more accurate than the former, it is time-consuming, especially, in the presence of an intense field, to optimize the MOs and expansion coefficients of the configuration state functions in the MCSCF method.

The lowest two states, $^2B_2$ and $^2A_2$ in bent CO_2^+, correlating to the ground state $^2\Pi_g$ at a linear geometry, are described by using the state-averaged MCSCF method. For CO_2^{2+}, the lowest three states, the ground triplet state $^3B_1$ ($^3\Sigma_g$ at a linear geometry) and the lowest two singlet states $^1A_1$ and $^1B_1$ ($^1\Delta_g$), must be considered. The lowest two singlet states of CO_2^{2+} are described by the state-averaged MCSCF method. The MOs are optimized separately for each spin multiplicity. The MCSCF active spaces of CO_2^+ and CO_2^{2+} include all valence orbitals and valence electrons. The adiabatic energy at an instantaneous field strength is calculated by the above CI method or the MCSCF.

4. Results and Discussion

We now apply the electrostatic model in section 2 to the CO_2 case. Consider a linear molecule $O^{P+}C^{Q+}O^{Z+}$ in a field ϵ. As suggested by the following numerical calculations, we assume that the charge on C does not change. The electrostatic energy of the expected ionic state $O^{(P-1)+}C^{Q+}O^{(Z+1)+}$ is then given by

$$E_I = I_p(O^{Z+}) - I_p(O^{(P-1)+}) - (Z + 1 - P)/2R - 2R\epsilon \quad (4)$$

where R is the C−O nuclear distance and I_p represents the ionization potential of the species (the reference energy is that of the initial state $O^{P+}C^{Q+}O^{Z+}$). The O atom with charge $P - 1$ is assumed to be in the descending well. As in eq 3, we estimate the intensity required for the creation of the charge-transfer ionic state by using the crossing condition $E_I = 0$:

$$\epsilon_c = [I_p(O^{Z+}) - I_p(O^{(P-1)+}) - (Z + 1 - P)/2R]/2R \quad (5)$$

Intramolecular charge transfer is considered a necessary condition for tunnel ionization. We assume that an appreciable amount of charge is transferred between the O atoms when the field strength exceeds the value given by eq 5. The degree of charge transfer is also estimated by the Mulliken population analysis of adiabatic states. With the help of eq 5 and the electrostatic consideration developed in section 2, we examine tunnel ionization of CO_2, CO_2^+, and CO_2^{2+} before Coulomb explosions.

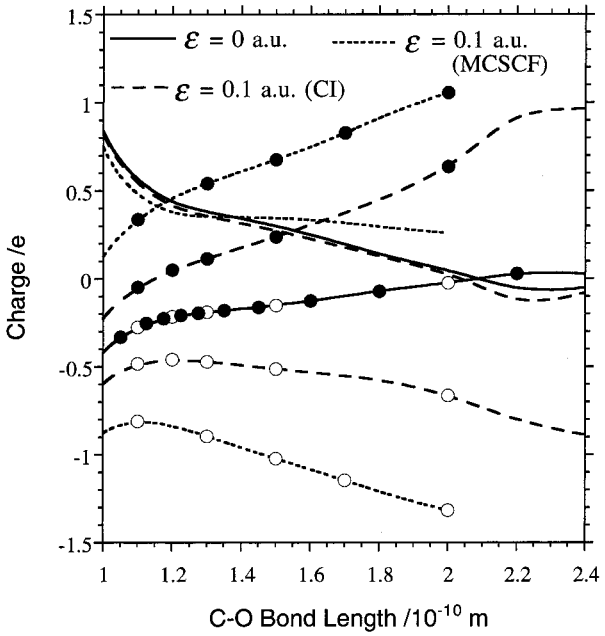

Figure 1. Charges on the three atoms in the *lowest adiabatic state* of linear CO_2 as functions of the C−O bond distance R (under symmetric stretching). The charge distribution is obtained by the Mulliken population analysis of the ab initio MO calculation. The polarization direction of the laser field $\epsilon(t)$ is assumed to be parallel to the molecular axis. The results for two field strengths are presented: $\epsilon(t) = 0$ au (solid line) and 0.1 au (broken and dotted). The charge distributions denoted by the broken and dotted lines are obtained by the CI method and the MCSCF method, respectively. The lines with open circles denote the charge of the O atom in the descending well, the lines with closed circles denote the charge of the O atom in the ascending well, and the lines without marks denote the charge of C. While the charge on C changes very little with $\epsilon(t)$, electron transfer between the two O atoms is induced by the field.

(i) Neutral CO_2. The charges on the three atoms in the *lowest adiabatic state* of linear CO_2 are plotted in Figure 1 against the C−O distance R. The total charge is assigned to each atom by the Mulliken population analysis of the ab initio MO calculation. The charge distribution changes as a function of the field strength and R. The polarization direction of the laser field is assumed to be parallel to the molecular axis (y-direction). It has been known that molecules are aligned by a linearly polarized laser electric field.[38,39] The results for two field strengths are shown: $\epsilon(t) = 0$ au (solid line) and 0.1 au (broken and dotted). The charge distributions denoted by the broken and dotted lines are obtained by the CI method and the MCSCF method, respectively. The lines with open circles denote the charge of the O atom in the descending well, the lines with closed circles denote the charge of the O atom in the ascending well, and the lines without marks denote the charge of C.

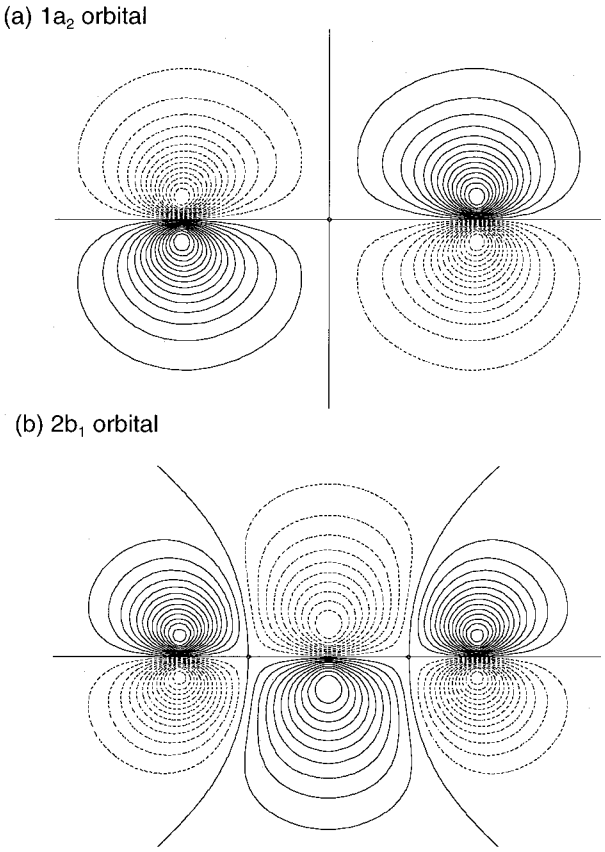

Figure 2. Shape of the nonbonding $1a_2$ HOMO and the antibonding $2b_1$ LUMO at the linear structure of $R = 1.2$ Å. The sign of the solid contour lines is opposite to that of the dotted lines. A linear combination of the two MOs forms an asymmetric charge distribution between the two O atoms, which characterizes the electron transfer and structure deformation of CO_2 in an intense field.

Near the equilibrium internuclear distance $R_e \approx 1.2$ Å, the charges of O and C at zero field are -0.22 and $+0.45$, respectively, as shown in Figure 1. The main charge distribution at zero field is expressed as $O^{0+}C^{0+}O^{0+}$. When a field is applied, an appreciable amount of negative charge is transferred from the O in the ascending to the O in the descending well; on the other hand, the net charge on C changes very little. Figure 1 shows that the charges of the two O atoms at $\epsilon(t) = 0.1$ au are -0.46 and $+0.05$ for the CI method and -0.83 and $+0.46$ for the MCSCF.

Charge transfers from O to O mainly through π orbitals. The key factor is the large transition moment between the nonbonding $1a_2$ HOMO and the antibonding $2b_1$ LUMO which is proportional to R. The HOMO and LUMO optimized at a linear geometry are shown in Figure 2. The $2b_1$ orbital lowers in energy for bending from a linear structure. However, the lowest adiabatic state in a field is not a pure excited state corresponding to the transition $1a_2 \rightarrow 2b_1$ but is rather characterized by a coherent superposition of $1a_2$ and $2b_1$. The linear combination of the two MOs produces an asymmetric charge distribution between the two O atoms, which mainly determines the electron transfer and structure deformation of CO_2 in an intense field. The differences in the optimized MO shapes between the neutral case and the cation cases are indiscernibly small, although atomic orbitals in an MO shrink only a little as the molecular charge increases.

In a weak field regime, the dipole moment is proportional to $\alpha_{yy}\epsilon(t)$, and the energy shift ΔE of the ground state by an applied field $\epsilon(t)$ follows the form $-\alpha_{yy}\epsilon^2(t)/2$, where α_{yy} is the molecular axis component of the polarizability. The lowest state energy calculated by the MCSCF method is always lower than the CI energy. The polarizability α_{yy} can be obtained by fitting the calculated value ΔE to $-\alpha_{yy}\epsilon^2(t)/2$. The value α_{yy} calculated by the MCSCF agrees with the experimentally observed value 4.1×10^{-24}/cm^3 (28 au), while the CI value is about half of the experimental value. This is a piece of evidence that the MCSCF is more accurate than the CI. The inaccuracy of the CI method results in insufficient charge transfer, as shown in Figure 1.

As R or $\epsilon(t)$ increases, the difference in charge between the O atoms increases. For $\epsilon(t) \geq 0.13$ au, a pure ionic structure $O^-C^{0+}O^+$ is formed at $R_e \approx 1.2$ Å if the process is adiabatic (the MCSCF calculation indicates that $\epsilon(t) \approx 0.13$ au is required for complete one-electron transfer between the two O atoms at $R \approx 1.2$ Å). The field strength necessary for the creation of $O^-C^{0+}O^+$ from $O^{0+}C^{0+}O^{0+}$ is estimated by eq 5 as

$$\epsilon_c = [(13.61 - 1.47)/27.21 - 1/2R]/2R \qquad (6)$$

where $I_p(O) = 13.61$ eV and $I_p(O^-) = 1.47$ eV are used. Near $R_e = 1.2$Å, $\epsilon_c = 0.05$ au. At $\epsilon_c = 0.05$ au, the charge of the O atom in the descending well is -0.5 for the MCSCF. This indicates that the ionic structure $O^-C^{0+}O^+$ becomes dominant as going beyond ϵ_c, as suggested by the dotted lines in Figure 1.

As mentioned in section 2, it is not just the population of the localized ionic state that determines the ionization probability. The attractive force due to the positively charged atom exerted on the localized ionic component determines how much portion is ionized out of the created ionic component. To estimate the effect of the positively charged atom on tunnel ionization, we refer to the H_2 at internuclear distance $R_{H-H} \approx 2$ Å. Since $R_{H-H} \approx 2$ Å is as long as the distance between the positive and negative charges in $O^-C^{0+}O^+$ ($\approx$2.3 Å), the positively charged atom in the H_2 at $R_{H-H} \approx 2$ Å exerts nearly the same attractive force on the localized ionic component as in the neutral CO_2 case. Although the ionization potential of the localized ionic component H^- is smaller than that of O^-, the difference is negligible: both H^- and O^- are extremely unstable in the intense field case. One can therefore assume that the positively charged atom in the H_2 at $R_{H-H} \approx 2$ Å has the same effect on tunnel ionization as in the neutral CO_2 case.

The ionization potential of H atom is nearly equal to that of O: CO_2 and the H_2 at $R_{H-H} \approx 2$ Å have nearly the same ϵ_c value. The efficiency of electron transfer in the H_2 at $R_{H-H} \approx 2$ Å is as high as in the neutral CO_2 case; for instance, at $\epsilon(t) \approx 0.09$ au, the population of the created ionic component of the H_2 at $R_{H-H} \approx 2$ Å is larger than 0.64 (the electron transfer takes place through the lowest adaiabatic state of H_2) and that of CO_2 is $\sim$0.77 (0.83 at $\epsilon(t) \approx 0.1$ au, as shown in Figure 1). Besides, the ionization potential of CO_2, 13.8 eV, is also close to the value of H_2 at $R_{H-H} \approx 2$ Å, i.e., 12.8 eV. We hence regard the H_2 at $R_{H-H} \approx 2$ Å as a reference molecule to estimate the intensity required for ionization of CO_2, though the total number of electrons of CO_2 is largely different from that of H_2. A wave packet simulation for the H_2 tells us that the field intensity required for ionization is around 0.08 au ($> \epsilon_c = 0.06$ au for the H_2 at $R_{H-H} \approx 2$ Å).[17] We thus expect for CO_2 that tunnel ionization via the ionic structure occurs somewhere not far above its $\epsilon_c = 0.05$ au (say, $\sim$0.08 au).

We examine how the potential surface of the lowest adiabatic state of linear CO_2 depends on the field strength. Four cases are drawn in Figure 3; $\epsilon(t) = 0$ au (solid line), CI calculation at $\epsilon(t) = 0.1$ au (broken), MCSCF calculation at $\epsilon(t) = 0.1$ au

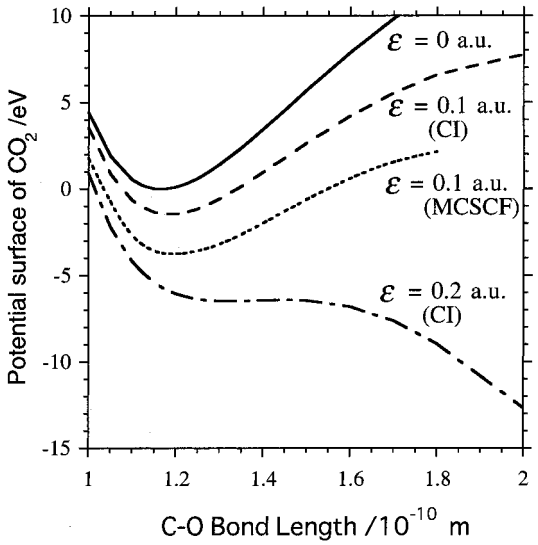

Figure 3. Potential surfaces of the lowest adiabatic state of linear CO_2 at three field strengths (under symmetric stretching): $\epsilon(t) = 0$ au (solid line), CI calculation at $\epsilon(t) = 0.1$ au (broken), MCSCF calculation at $\epsilon(t) = 0.1$ au (dotted), and CI calculation at $\epsilon(t) = 0.2$ au (dash−dotted). The potential surface calculated by the CI is higher than the MCSCF result because of insufficient charge transfer in the CI calculation.

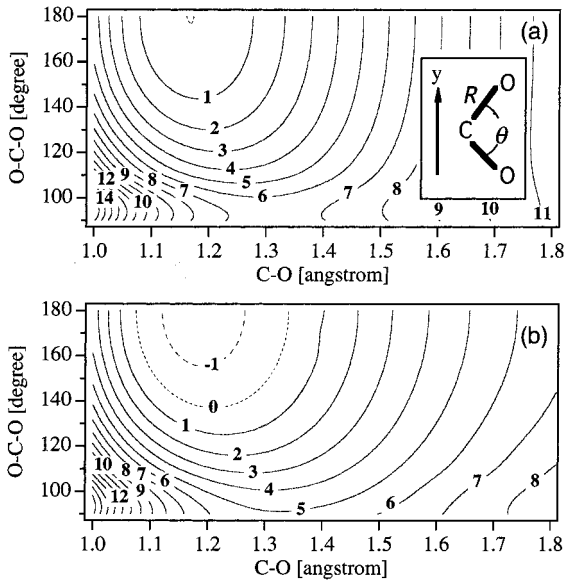

Figure 4. 2D Potential surfaces of the lowest adiabatic state of CO_2 as a function of the C−O distance R and the O−C−O bending angle θ: (a) $\epsilon(t) = 0$ and (b) 0.1 au. C_{2v} symmetry is assumed. The adiabatic energies are calculated by the CI method. The heights of contour lines are indicated in units of eV. The linear structure at ∼1.2 Å is stable. The orientation of the O−O axis is assumed to be parallel to the polarization direction y of the electric field as shown in the inset.

(dotted), and CI calculation at $\epsilon(t) = 0.2$ au (dash−dotted). As the field strength increases from 0 to 0.1 au ($>\epsilon_c$) the dissociation energy is reduced from 15 to 10 eV in the CI case and to 8 eV in the MCSCF case. The overall shape of the potential surface is, however, nearly the same as that at zero field. The linear structure of $R_e = 1.2$ Å is stable as in the field-free case and a field intensity that is larger than ∼0.15 au is required for dissociation.

Both MCSCF and CI methods qualitatively agree with each other; the polarizability calculated is a quadratic increasing function of R and the charge transferred between the two O atoms is more or less given by a linear increasing function of R. The most notable quantitative difference is that the potential surface calculated by the CI is higher than the more accurate MCSCF result because of insufficient charge transfer in the CI calculation. As R increases, the difference between the CI and MCSCF results increases. As a result, the dissociation energy at a nonzero field is overestimated in the CI calculation.

The potential surfaces of the lowest adiabatic state at $\epsilon(t) = 0$ and 0.1 au calculated by the CI method are drawn in Figure 4 as a function of R and the bond angle θ (under C_{2v} symmetry). Although the 2D potential at a nonzero field is shifted down at any structure in comparison with that at zero field, the overall *shape* of the 2D potential surface at $\epsilon(t) = 0.1$ au is nearly the same as that at zero field. The contour map shows that a stable linear structure exists even at field strengths $\epsilon(t) \approx 0.1$ au. Around $R_e = 1.2$ Å, the curvature of the more reliable MCSCF potential with respect to θ is nearly equal to that of the CI potential. One cannot expect large amplitude bending motion at $\epsilon(t) = 0.1$ au. In the neutral stage, ionization to CO_2^+ hence occurs before the field intensity becomes large enough to deform the neutral CO_2.

Ab initio MO calculations show that the curvature of the potential with θ is larger at nonzero fields than at zero field. The angle dependence of the potential can be understood as follows. Using the charge transferred between the two O atoms, $C_{O\to O}$, we express the induced dipole $\alpha|\epsilon(t)|$ as $C_{O\to O}R_{O-O}$, where $R_{O-O} = 2R \sin(\theta/2)$ is the distance between the two O atoms. See the inset in Figure 4. The field-induced energy shift $-\alpha\epsilon^2(t)/2$ can thus be given by $-C_{O\to O}R|\epsilon(t)| \sin(\theta/2)$. From ab initio MO calculations, we have found that the transferred charge $C_{O\to O}$, which is a linear increasing function of R and $|\epsilon(t)|$, is nearly independent of θ. At a fixed R, the absolute magnitude of the field-induced energy shift, $C_{O\to O}R|\epsilon(t)| \sin(\theta/2)$, is smaller for bending. This is attributed to the feature that the transition moment between the $1a_2$ HOMO and $2b_1$ LUMO decreases for bending. In other words, as R_{O-O} decreases for bending, the induced dipole of the lowest adiabatic state which shifts the energy down becomes smaller.

We can now separate the 2D potential surface $E(R,\theta;\epsilon(t))$ into three parts:

$$E(R,\theta;\epsilon(t)) = E(R,\theta;\epsilon(t)=0) - C_{O\to O}R|\epsilon(t)| + C_{O\to O}R|\epsilon(t)|[1 - \sin(\theta/2)] \quad (7)$$

where the second term $-C_{O\to O}R|\epsilon(t)|$ represents the field-induced energy shift at the linear structure and the last term represents the angle dependence of the field-induced energy shift (which in general hinders the bending motion for a fixed R). Equation 7 explains the angle dependence of the 2D potential calculated by the CI or MCSCF method. For $R = 1.2$ Å, $\theta = 180°$, and $\epsilon(t) = 0.1$ au, we use the value $C_{O\to O} \sim 0.25$ estimated from the Mulliken population analysis for the CI case; the expression proposed for the field-induced energy shift, $C_{O\to O}R|\epsilon(t)|$, provides a value close to the calculated shift 1.5 eV in Figure 3 (the difference between the zero field case and the CI case for $\epsilon(t) = 0.1$ au). The angle dependence of the field-induced energy shift is then very small as $C_{O\to O}R|\epsilon(t)|[1 - \sin(\theta/2)] \approx 0.2$ eV at $\theta = 120°$. Around $R_e = 1.2$ Å, the curvature of the potential with θ is nearly independent of the field strength.

The more reliable MCSCF potential is much lower than the CI potential in Figure 4. The change in the potential along θ is generally steeper in the MCSCF case than in the CI case. Around $R_e = 1.2$ Å, however, both potentials have nearly the same curvature with θ. For $R = 1.2$ Å and $\epsilon(t) = 0.1$ au, the value of $C_{O\to O}$ obtained by the MCSCF is ∼0.6. The difference in the angle dependence $C_{O\to O}R|\epsilon(t)|[1 - \sin(\theta/2)]$ between the

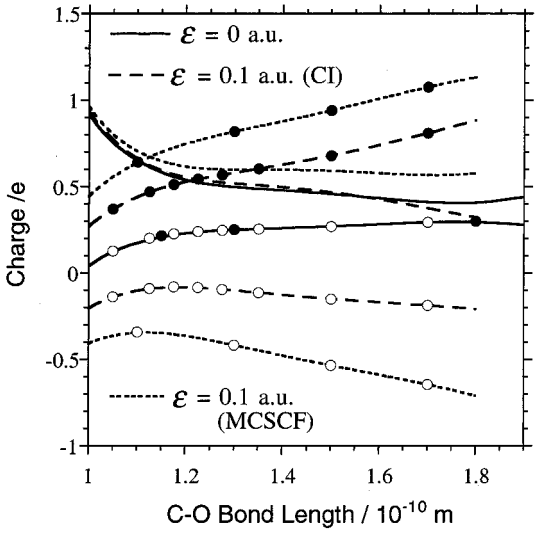

Figure 5. Charges on the three atoms in the lowest adiabatic state of linear CO_2^+ as functions of the C−O distance R (under symmetric stretching). The notations are the same as used in Figure 1.

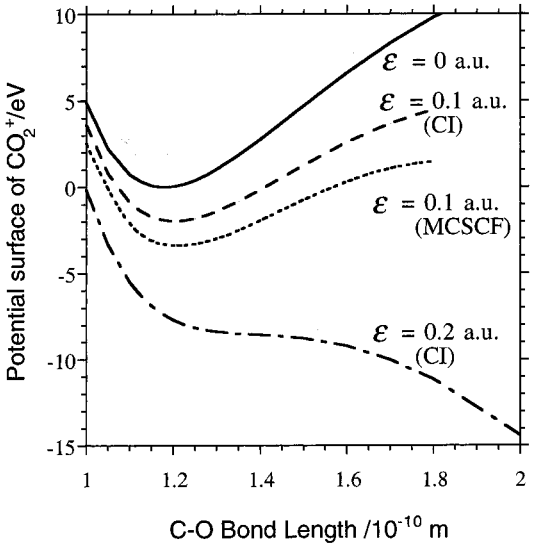

Figure 6. Potential surfaces of the lowest adiabatic state of linear CO_2^+ at three field strengths (under symmetric stretching). The notations are the same as in Figure 3. The dissociation energy is smaller than the corresponding one in the neutral CO_2 case, but still as large as ∼5.5 eV at $\epsilon(t) = 0.1$ au, as shown by the dotted line.

MCSCF and CI potentials is then small as 0.3 eV at $\theta = 120°$. The difference in the curvature between them is thus small. Near R_e, therefore, the electric field hardly induces large amplitude bending motion because it does not flatten the potential along θ.

(ii) CO_2^+. The charges on the three atoms in the lowest adiabatic state ($^2\Pi_g$ state) of linear CO_2 are plotted in Figure 5. For the ground electronic state of CO_2^+ at zero field, the equilibrium structure is linear and $R_e \approx 1.2$ Å. Around R_e, as shown in Figure 5, the charges of O and C are +0.23 and +0.55, respectively. The main charge distribution at zero field is expressed as $O^{0+}C^{+}O^{0+}$. As R or $\epsilon(t)$ increases, the difference in charge between the O atoms increases. The minimum field strength required for the creation of $O^{-}C^{+}O^{+}$ is $\epsilon_c = 0.05$ au at $R \approx 1.2$ Å. For $\epsilon(t) = 0.1$ au ($>\epsilon_c$), the difference in charge between the two O atoms at $R \approx 1.2$ Å is 0.6 for CI and 1.1 for MCSCF; thus, an ionic component $O^{-}C^{+}O^{+}$ is created from $O^{0+}C^{+}O^{0+}$. The net charge on C changes very little as in the neutral case.

In addition to the positive charge of O^+, the charge of the C^+ strongly pulls back the electron escaping from the O^- in the descending well. To quantify the role of C^+ in the ionization process and the intensity required for ionization of the created ionic component $O^{-}C^{+}O^{+}$, we employ a 1D model of linear H_3^+ where the two electrons are allowed to move only along the molecular axis.[40] We fix R_{H-H} at 1.2 Å so that the positively charged atoms in the H_3^+ molecule have the same effect on tunnel ionization as in the CO_2^+ case. Using the ionization potentials of the 1D model atoms, I_p(1D H) = 18 eV and I_p(1D H^-) = 1.6 eV, we obtain $\epsilon_c = 0.075$ au for the crossing from $H^{0+}H^{+}H^{0+}$ to $H^{-}H^{+}H^{+}$. By numerically solving the time-dependent Schrödinger equation of the 1D H_3^+ (λ = 700−1000 nm), we find that for this system tunnel ionization sets in when the field strength approaches 0.1 au. This value is a little larger than $\epsilon_c = 0.075$ au for 1D H_3^+. Since $\epsilon_c = 0.05$ au of CO_2^+ at $R \approx 1.2$ Å is smaller than 0.075 au for the 1D H_3^+ and the internuclear distance $R \approx 1.2$ Å of CO_2^+ is equal to R_{H-H}, we conclude that the threshold field strength for ionization of CO_2^+ at $R \approx 1.2$ Å is less than or somewhere around 0.1 au. This conclusion is in accord with the fact that the ionization potential of CO_2^+ (∼23 eV) is smaller than that of the 1D H_3^+ (∼28 eV).

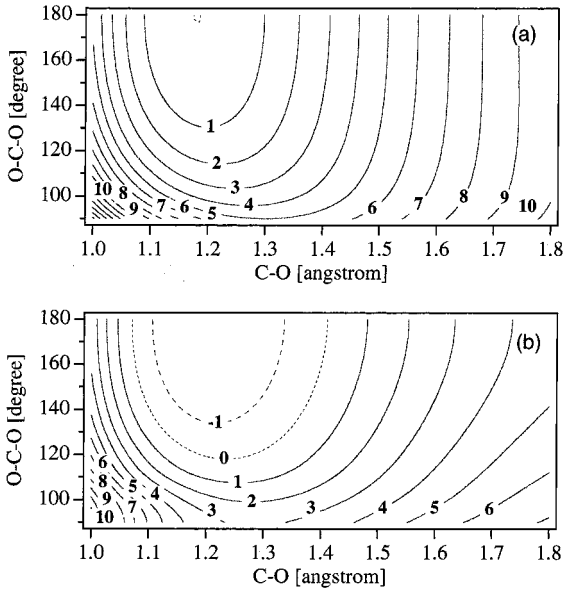

Figure 7. 2D Potential surfaces of the lowest adiabatic state of CO_2^+ calculated by the CI method: (a) $\epsilon(t) = 0$ and (b) $\epsilon(t) = 0.1$ au. C_{2v} symmetry is assumed. The heights of contour lines are indicated in units of eV. The linear structure at ∼1.2 Å is stable.

The potential surface of the lowest adiabatic state of linear CO_2^+ is presented in Figure 6 for three field strengths (under symmetric stretching). The dissociation energy at each field strength is smaller than the corresponding one in the neutral case, but still as large as 5.5 eV at $\epsilon(t) = 0.1$ au for the MCSCF calculation (∼7 eV for CI). While ionization is expected to occur around $\epsilon(t) = 0.1$ au, the bond stretching will be small at this strength.

We have also examined the bending motion by calculating the 2D potential surfaces of the lowest two adiabatic states (connected with close lying $^2B_2$ and $^2A_2$ states at zero field) at various field strengths. The 2D surfaces of the lowest adiabatic state at $\epsilon(t) = 0$ and 0.1 au are shown in Figure 7 (the lowest adiabatic state is connected with $^2B_2$ at zero field). The potential curvature of CO_2^+ with θ is smaller than that of CO_2. Around $R_e \approx 1.2$ Å, the calculated frequency for the bending mode of

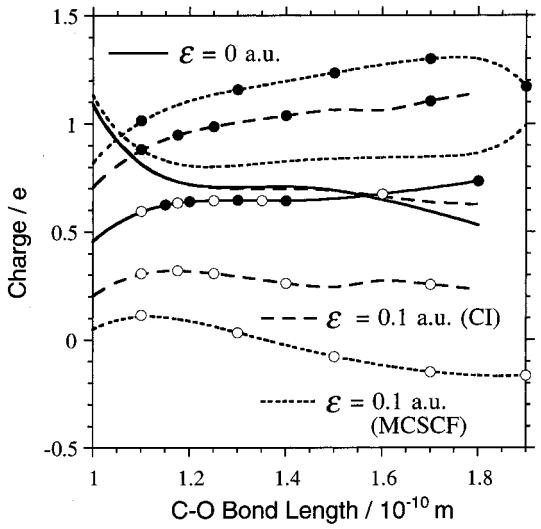

Figure 8. Charges on the three atoms in the lowest singlet state of linear CO_2^{2+} as functions of C−O distance R (under symmetric stretching). The notations are the same as in Figure 1.

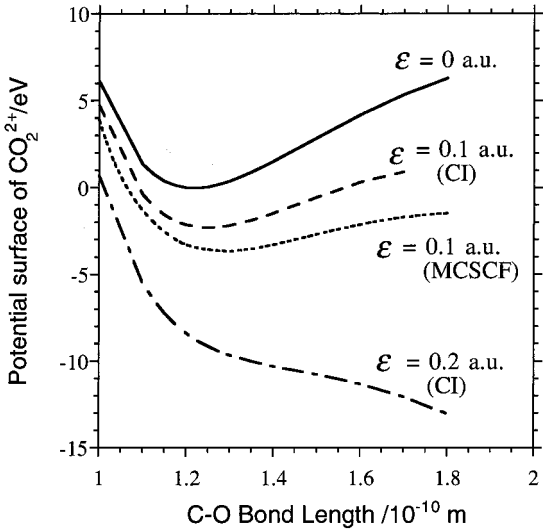

Figure 9. Potential surfaces of the lowest singlet state of linear CO_2^{2+} at three field strengths (under symmetric stretching). Bond stretching occurs at field strengths that are weaker than the strength $\epsilon_c = 0.18$ au required for tunnel ionization.

CO_2^+ at zero field is $^7/_{10}$ths as large as that of CO_2; the mean amplitude for bending motion increases only $1/\sqrt{0.7} \approx 1.2$ times as going from CO_2 to CO_2^+.

Around R_e, the shape of the potential surface changes only a little up to $\epsilon(t) = 0.1$ au, indicating that large amplitude bending motion is not induced by such a field. The lowest two adiabatic states have nearly the same adiabatic potential surface (around the potential minimum, the difference is less than 0.5 eV).

For CO_2 and CO_2^+, in the ionization stage, the internuclear distance R is small: electron transfer will occur adiabatically in the time-dependent lowest adiabatic state (for CO_2^+, the lowest two states may be involved), as has been assumed above. The probabilities of nonadiabatic transitions to the other adiabatic states are expected to be small.

(iii) CO_2^{2+}. In the subsequent stage of the ionization of CO_2^+, one must consider at least the lowest three adiabatic states of CO_2^{2+}, the ground triplet state connected with the $^3B_1$ state at zero field and the nearly degenerate lowest singlet states connected with $^1A_1$ and $^1B_1$ at zero field ($^1\Delta_g$ at a linear geometry). The energy difference between $^1A_1$ and $^3B_1$ at zero field is small as ∼1.5 eV near the equilibrium geometry ($R_e \approx$ 1.2 Å and $\theta = 180°$) and the potential surfaces of the lowest three states have nearly the same shape, irrespective of the field strength. Considering the strong intensity of the laser field, the difference of ∼1.5 eV is not decisive in nuclear dynamics. The discussion below applies to both singlet and triplet cases.

The charges on the three atoms in the lowest singlet state of linear CO_2^{2+} (connected with $^1\Delta_g$ at zero field) are plotted in Figure 8. The charge distribution for the ground triplet state is nearly identical with that in Figure 8. Two positive charges in CO_2^{2+} are nearly equally distributed among the three atoms. We therefore consider three configurations $O^{0+}C^+O^+$, $O^+C^+O^{0+}$, and $O^+C^{0+}O^+$. An ionic structure favorable for tunnel ionization is the $O^-C^+O^{2+}$ created from $O^{0+}C^+O^+$. The field strength required for this crossing estimated by eq 5 is $\epsilon_c = 0.18$ au at $R \approx 1.2$ Å, which is expected to be the minimum intensity for tunnel ionization. As shown in Figure 8, near R_e, the charge of the O atom in the descending well is nearly zero at $\epsilon(t) = 0.1$ au (see the MCSCF value); the main structure at $\epsilon(t) = 0.1$ au is $O^{0+}C^+O^+$. In the intensity region up to $\epsilon(t) \approx 0.1$ au, the electron transfer corresponds to the transition from $O^+C^+O^{0+}$ to $O^{0+}C^+O^+$ (the energy of the latter structure is always lower than the former one when $\epsilon(t) > 0$). Much higher field strengths (∼0.2 au) are required to create the ionic structure favorable for tunnel ionization, $O^-C^+O^{2+}$.

Direct ionization from $O^{0+}C^+O^+$ may be possible. We have solved the time-dependent Schrödinger equation for a 3D linear H_3^{2+} at $R_{H-H} \approx 1.2$ Å designed after CO_2^{2+} at $R \approx 1.2$ Å. Tunnel ionization proceeds via $H^{0+}H^+H^+$; the field strength required for tunnel ionization is found to be about 0.2 au. We hence conclude that tunnel ionization of CO_2^{2+} at its equilibrium internuclear distance requires at least a field strength of $\epsilon_c =$ 0.18 au.

The potential surface of linear CO_2^{2+} in the lowest singlet state (connected with $^1\Delta_g$ at zero field) is presented in Figure 9 for three field strengths. As shown by the MCSCF result, the dissociation energy is as small as ∼2.5 eV at $\epsilon(t) = 0.1$ au. The potential surface becomes dissociative for $\epsilon(t) > 0.11$ au. The bond of CO_2^{2+} is stretched at field strengths 0.11−0.18 au, which do not cause tunnel ionization near R_e.

In Figure 10, we show 2D potential surfaces of the lowest singlet adiabatic state of CO_2^{2+} for three field strengths: (a) $\epsilon(t) = 0$, (b) 0.1, and (c) 0.2 au. These three potential surfaces, which are adiabatically connected with $^1A_1$ at zero field, are calculated by the CI method. Around $R_e = 1.2$ Å, the calculated frequency for the bending mode of CO_2^{2+} at zero field is $^6/_{10}$-ths as large as that of CO_2; the mean amplitude for bending motion increases only $1/\sqrt{0.6} \approx 1.3$ times on going from CO_2 to CO_2^{2+}. The experimentally observed large amplitude bending motion cannot be simply attributed to the structure change between CO_2 and CO_2^{2+} at zero field.

As mentioned in the subsection on CO_2, if R were fixed, bending would be more hindered by an electric field. However, for field strengths >0.11 au, the bond stretches. Figure 10c demonstrates that an isoenergy contour line does not make a half-circle as in Figure 4. Along isoenergy contour lines starting from the equilibrium structure, the nuclear wave packet spreads. A typical case is indicated in Figure 10c by the stream of arrows, which determines the maximum amplitude for the instantaneous potential. Another important factor that increases the bending amplitude as R increases comes from the fact that the potential at zero field is very flat against θ for $R > 1.5$ Å, as shown in Figure 10a. When the absolute value of the field strength is large and when it is small, the amplitude of bending motion on an instantaneous potential hence becomes larger in the large R

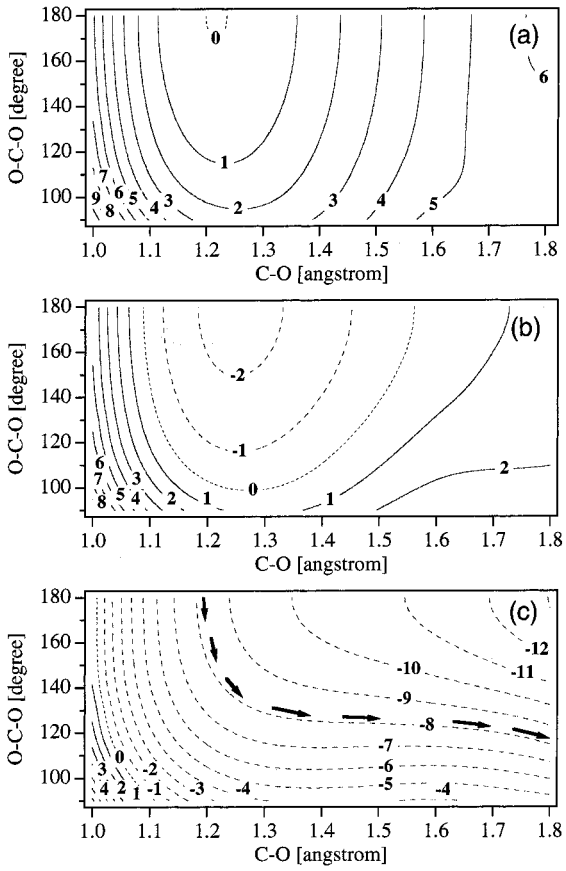

Figure 10. 2D Potential surfaces of the lowest singlet state (connected with $^1A_1$ at zero field) of CO_2^{2+} at (a) $\epsilon(t) = 0$, (b) 0.1, and (c) 0.2 au calculated by the CI method. The heights of contour lines are indicated in units of eV. As shown in Panel (c), when the absolute value of the field strength is large, the bending motion becomes less hindered as R increases. A typical 2D motion is indicated by the stream of arrows. The potential at zero field is very flat against θ for $R > 1.5$ Å as shown in Panel (a), which also increases the bending amplitude as R increases.

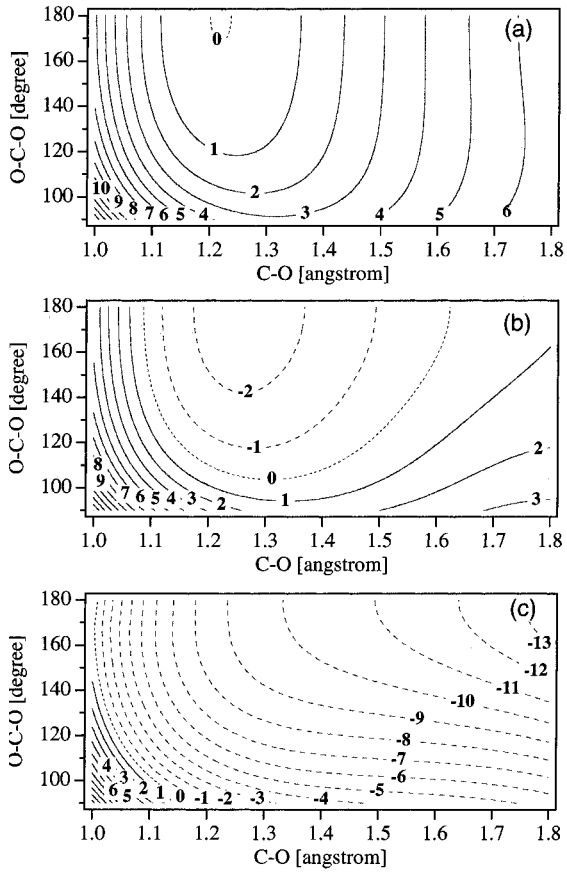

Figure 11. 2D Potential surfaces of the ground triplet state of CO_2^{2+} at (a) $\epsilon(t) = 0$, (b) 0.1, and (c) 0.2 au calculated by the CI method. The triplet state potential surface is lower in absolute energy than the lowest singlet state by ~1.5 eV.

region. We thus expect that bond stretching triggers a large amplitude bending motion, as observed experimentally.

2D adiabatic potential surfaces of the ground triplet state of CO_2^{2+} are shown in Figure 11. Comparing Figures 10 and 11, one finds that the difference in potential shape between the ground triplet state and the lowest two singlet states is small. The nuclear wave packet dynamics on the ground triplet state is expected to be nearly the same as those on the lowest two singlet states.

The change in the potential along θ is steeper in the more reliable MCSCF case than in the CI case. For $R = 1.8$ Å and $\epsilon(t) = 0.2$ au, the difference in the angle dependence $C_{O\rightarrow O}R|\epsilon(t)|[1 - \sin(\theta/2)]$ between the MCSCF and CI potentials is 1−1.5 eV at $\theta = 120°$. Although the bending amplitude in the MCSCF potential is probably smaller than in the CI potential, the difference between the two potentials does not change the present qualitative discussion.

The value of ϵ_c decreases with increasing R. For instance, $\epsilon_c = 0.14$ au at $R \approx 1.8$ Å. As R increases, the attractive force due to the distant nuclei C^+ and O^{2+} in the ionic structure $O^-C^+O^{2+}$ becomes weaker against an electron in O^-. Once an ionic component of $O^-C^+O^{2+}$ is created at large R when the field intensity reaches ϵ_c, ionization therefore occurs at a high probability. There is a possibility that when R is large the population of the ionic component created is smaller than the value expected for the adiabatic electron transfer between the O atoms. We, however, expect that an electron transfers adiabatically from O to O even near $R = 1.8$ Å because of the intervention of the C atom.

In the neutral and monocation stages of CO_2, ionization occurs before the field intensity becomes large enough to deform the molecule. In the dication stage, laser-induced bond stretching is accompanied by large amplitude bending motion, which is responsible for the observed geometrical structure of Coulomb explosion species CO_2^{3+}, namely, that the C−O bond length is stretched to about 1.6 Å with a large mean amplitude of bending motion.

Acknowledgment. This work was supported in part by the Development of High-Density Optical Pulse Generation and Advanced Material Control Techniques and by a grant-in-aid for scientific research from the Ministry of Education, Science, and Culture, Japan (12640484). We express our appreciation to Professor K. Yamanouchi and Professor A. Hishikawa for discussion of their work. H.K. thanks Professor T. T. Nguen-Dang for discussions on molecular orbitals in intense laser fields.

References and Notes

(1) Lin, S. H.; Fujimura, Y.; Neusser, H. J.; Schlag, E. W. *Multiphoton Spectroscopy of Molecules*; Academic Press: London, 1984.

(2) Gavrila, M., Ed. *Atoms in Intense Fields;* Academic Press: NewYork, 1992.

(3) Eberly, J. H.; Javanainen, J.; Rzazewski, K. *Phys. Rep*. **1991**, *204*, 331. Lewenstein, M.; Kulander, K. C.; Schafer, K. J.; Bucksbaum, P. H. *Phys. Rev. A* **1995**, *51*, 1495.

(4) Keldysh, L. V. *Sov. Phys. JETP* **1965**, *20*, 1307. Faisal, F. H. M. *J. Phys. B* **1973**, *6*, L89. Augst, S.; Meyerhofer, D. D.; Strickland, D.; Chin, S. L. *J. Opt. Soc. Am. B* **1991**, *8*, 858. Ammosov, M. V.; Delone, N. B.; Krainov V. P. *Sov. Phys. JETP* **1986**, *64*, 1191.

(5) Krainov, V. P.; Reiss, H. R.; Smirnov, B. M. *Radiative Processes in Atomic Physics*; Wiley: New York, 1997.

(6) Posthumus, J. H.; Giles, A. J.; Thompson, M. R.; Codling, K. *J. Phys. B* **1996**, *29*, 5811. Constant E.; Stapelfelt, H.; Corkum, P. B. *Phys. Rev. Lett.* **1996**, *76*, 4140. Codling, K.; Frasinski, L. J. *J. Phys. B* **1993**, *26*, 783. Schmidt, M.; Normand, D.; Cornaggia C. *Phys. Rev. A* **1994**, *50*, 5037.

(7) Kou, J.; et al. *J. Chem. Phys.* **2000**, *112*, 5012.

(8) Sanderson, J. H.; El-Zein, A.; Bryan, W. A.; Newell, W. R.; Langley, A. J.; Taday, P. F. *Phys. Rev. A* **1999**, *59*, R2567.

(9) Hishikawa, A.; Iwamae, A.; Yamanouchi, K. *J. Chem. Phys.* **1999**, *111*, 8871.

(10) Cornaggia, C. *Phys. Rev. A* **1993**, *54*, R2555.

(11) Hishikawa, A.; Iwamae, A.; Yamanouchi, K. *Phys. Rev. Lett.* **1999**; *83*; 1127.

(12) Ledingham, K. W. D.; et al. *J. Phys. Chem. A* **1998**, *102*, 3002.

(13) Zuo, T.; Bandrauk, A. D. *Phys. Rev. A* **1993**, *48*, 3837; **1995**, *52*, R2511.

(14) Seidemann, T.; Ivanov, M. Y.; Corkum, P. B. *Phys. Rev. Lett.* **1995**, *75*, 2819.

(15) Bandrauk, A. D. *Comments At. Mol. Phys.* D **1999**, *1*, 97.

(16) Yu, H.; Zuo, T.; Bandrauk, A. D. *Phys. Rev. A* **1996**, *54*, 3290.

(17) Harumiya, K.; Kawata, I.; Kono, H.; Fujimura, Y. *J. Chem. Phys.* **2000**, *113*, 8953.

(18) (a) Kawata, I.; Kono, H.; Fujimura, Y. *J. Chem. Phys.* **1999**, *110*, 11152. Kawata, I.; H. Kono; Fujimura, Y. *Chem. Phys. Lett.* **1998**, *289*, 546. (b) Kono, H.; Kawata, I. In *Advances in Multi-Photon Processes and Spectroscopy*; Gordon, R. J.; Fujimura, Y. Eds.; World Scientific: Singapore, 2001; Vol. 14, p 165.

(19) Mittleman, M. H. *Introduction to the Theory of Laser-Atom Interactions*, 2nd ed.; Prenum: New York, 1993.

(20) Zavriyev, A.; Bucksbaum, P. H.; Squier, J.; Saline, F. *Phys. Rev. Lett.* **1993**, *70*, 1077.

(21) Walsh, T. D. G.; Ilkov, F. A.; Chin, S. L.; Châteauneuf, F.; Nguyen-Dang, T.-T.; Chelkowski, S.; Bandrauk, A. D.; Atabek, O. *Phys. Rev. A* **1998**, *58*, 3922. Nguyen-Dang, T.-T.; Châteauneuf, F.; Manoli, S.; Atabek, O.; Keller, A. *Phys. Rev. A* **1997**, *56*, 2142.

(22) Bandrauk, A. D. *Molecules in Intense Laser Fields*; M. Dekker: New York, 1994; Chapters 1−3.

(23) Dietrich, P.; Ivanov, M. Yu.; Ilkov, F. A.; Corkum, P. B. *Phys. Rev. Lett.* **1996**, *77*, 4150.

(24) Schmidt, M. W.; Baldridge, K. K.; Boatz, J. A.; Elbert, S. T.; Gordon, M. S.; Jensen, J. H.; Koseki, S.; Matsunaga, N.; Nguyen, K. A.; Su, S.; Windus, T. L.; Dupuis, M.; Montgomery, J. A., Jr. *J. Comput. Chem.* **1993**, *14*, 1347−1363.

(25) DeWitt, M. J.; Levis, R. J. *Phys. Rev. Lett.* **1998**, *81*, 5101. DeWitt, M. J.; Levis, R. J. *J. Chem. Phys.* **1998**, *108*, 7739.

(26) Kawata, I.; Kono, H.; Fujimura, Y.; Bandrauk, A. D. *Phys. Rev. A* **2000**, *62*, 031401(R). Kawata, I.; Bandrauk, A. D.; Kono, H.; Fujimura, Y. *Laser Phys.* **2001**, *11*, 188.

(27) Gibson, G. N.; Li, M.; Guo, C.; Nibarger, J. P. *Phys. Rev. A* **1998**, *58*, 4723.

(28) Bandrauk, A. D. In *The Physics of Electronic and Atomic Collisions*; Itikawa, Y., et al., Eds.; AIP Conf. Proc. 500; AIP: New York, 1999; p 102.

(29) Kono, H.; Kita, A.; Ohtsuki, Y.; Fujimura, Y. *J. Comput. Phys.* **1997**, *130*, 148.

(30) Kawata, I.; Kono, H. *J. Chem. Phys.* **1999**, *111*, 9498.

(31) Mulliken, R. S. *J. Chem. Phys.* **1939**, *7*, 20.

(32) Ionization rates of H_2^+ in static fields, as well as adiabatic energies, have been calculated by complex scaling methods. See, e.g.: Mulyukov, Z.; Pont, M.; Shakeshaft, R. *Phys. Rev. A* **1996**, *54*, 4299. Plummer, M.; McCann, J. F. *J. Phys. B* **1996**, *29*, 4625.

(33) Kawata, I.; Kono, H.; Fujimura, Y. To be published.

(34) Saenz, A. *Phys. Rev. A* **2000**, *61*, 051402 (R).

(35) Wolniewicz, L. *J. Chem. Phys.* **1993**, *99*, 1851.

(36) (a) Ruedenberg, K.; Schmidt, M. W.; Dombek, M. M.; Elbert, S. T. *Chem. Phys.* **1982**, *71*, 41, 51, 65. (b) Schmidt, M. W.; Gordon, M. S. *Annu. Rev. Phys. Chem.* **1998**, *49*, 233.

(37) Krishnan, R.; Binkley, J. S.; Seeger, R.; Pople, J. A. *J. Chem. Phys.* **1980**, *72*, 650. The orbital exponents of the polarization d functions for C and O are 0.626 and 1.292, respectively; the sp exponents of diffuse functions are set to 0.0438 (C) and 0.0845 (O).

(38) Friedrich, B.; Herschbach, D. *Phys. Rev. Lett.* **1995**, *74*, 4623. Larsen, J. J.; Sakai, H.; Safvan, C. P.; Wendt-Larsen, Ida; Stapelfeldt, H. *J. Chem. Phys.* **1999**, *111*, 7774.

(39) Schmidt, M.; Dobosz, S.; Meynadier, P.; D'Oliveira, P.; Normand, D.; Charron, E.; Suzor-Weiner, A. *Phys. Rev. A* **1999**, *60*, 4706.

(40) Yu, H.; Bandrauk, A. D. *Phys. Rev. A* **1997**, *56*, 685.